Reaktor

p-ISSN 0852 – 0798
e-ISSN 2407 – 5973

Website: http://ejournal.undip.ac.id/index.php/reaktor/

Reaktor, Vol. 26 No. 1, April Year 2026, pp. 1-10

Comparative Simulation and Modeling of Hydrogen Explosion Consequences Based on TNT Equivalent

Virda Nur Lu'lu [1,2)], Pramujo Widiatmoko [1,2)], Hary Devianto [1,2,*)]

[1)] Department of Chemical Engineering, Faculty of Industrial Technology, Institut Teknologi Bandung
Jalan Ganesha No.10, Bandung 40132, Indonesia
[2)]Laboratory of Energetic Process and Electrochemical Safety Laboratory, Institut Teknologi Bandung
Jalan Ganesha No.10, Bandung 40132, Indonesia

[*)] Corresponding author: hardev@itb.ac.id

(Received: 18 February 2026; Accepted: 18 June 2026; Published: 22 June 2026)

Abstract

Hydrogen is increasingly adopted as a low-carbon energy carrier, creating a need for rapid and auditable blast-consequence screening to inform hazard zoning. This study develops a web-based simulation platform that automates a transparent TNT-equivalent workflow with minimal inputs (inventory volume and evaluation distance). The platform converts volume to mass, estimates TNT-equivalent charge using an energy basis and efficiency factor, applies Hopkinson–Cranz cube-root scaling, and predicts peak side-on overpressure using three well-established empirical correlations (Crowl and Louvar, Alonso, and Sadovski) under harmonized assumptions, while exporting calculation logs for traceability. Validation uses a Type-IV high-pressure hydrogen vessel-burst dataset with measurements at 2–18 m. Over the sensor-intact 6–18 m window, the Alonso correlation achieves MAE 6.006 kPa with R^2 0.999, whereas Crowl and Louvar and Sadovski correlations yield MAEs of 18.136 kPa and 17.164 kPa with R^2 of 0.985 and 0.993. A 50 kg TNT-equivalent Gangneung 2019 case gives 50.9–86.7 kPa at 15 m and 3.58–6.34 kPa at 100 m, consistent with reported steel deformation and widespread glazing damage. Overall, the platform enables transparent, traceable preliminary consequence estimation to support hazard-zoning decisions for hydrogen storage.

Keywords: Blast consequence screening; Hopkinson–Cranz scaling; Hydrogen explosion; Peak side-on overpressure; TNT equivalent

How to Cite This Article: Lu'lu, V.N., Widiatmoko, P., and Devianto, H., (2026) Comparative Simulation and Modeling of Hydrogen Explosion Consequences Based on TNT Equivalent, Reaktor, 26 (1),82563, https://doi.org/10.14710/reaktor.82563

INTRODUCTION

Hydrogen (H_2) is increasingly positioned as a low-carbon energy carrier, accelerating the deployment of production, storage, distribution, and refuelling infrastructure (Ma et al., 2024). According to the latest global assessment, global hydrogen demand reached almost 100 Mt in 2024, while the use of low-emission hydrogen remained below 1% of total hydrogen demand (IEA, 2025). Looking ahead, DNV's 2026 hydrogen outlook projects that global hydrogen and derivatives supply will rise from approximately 100 MtH_2/yr in 2025 to about 130

MtH₂/yr by 2035, and further to nearly 280 MtH₂/yr by 2060 (DNV, 2026). The outlook is demand-anchored because near-term projects are expected to proceed only when credible, policy-supported offtake is available. In facility design and operation, this trend reinforces the need for rapid and defensible separation-distance decision-making and consequence screening, particularly where hydrogen assets are located near critical infrastructure and occupied areas (Joshi et al., 2024; LaChance, 2009).

Hydrogen explosion hazards remain central to process safety because hydrogen exhibits a wide flammability range in air from 4 to 75% by volume and a very low minimum ignition energy of about 0.02 mJ, meaning ignition can be initiated by weak ignition sources under certain mixing conditions (Calabrese et al., 2024; Suwa, 2024). Incident statistics further highlight the practical relevance of hydrogen safety, as the Hydrogen Incident Database reported 120 hydrogen incidents between 1999 and 2019. Based on incident-location statistics, these events were dominated by laboratory cases (38.3%), followed by refuelling stations (10.6%) and commercial facilities (9.0%) (Yang et al., 2021). The same study also reports incident-equipment statistics, showing that piping, fittings, and valves accounted for 32.28% of equipment-related incidents, while hydrogen storage equipment accounted for 15.51% (Yang et al., 2021). These location- and equipment-based statistics support the relevance of processing- and storage-related systems in hydrogen incident analysis, particularly chemical plants, refineries, production facilities, storage/use facilities, process piping, and hydrogen storage equipment. A notable large-scale example is the Gangneung incident (South Korea, May 2019), where a pressure-vessel system used for electrolyzer testing exploded with a reported blast equivalent of 50 kg TNT (CHS, 2019), resulting in two fatalities, six injuries, and severe damage to nearby facilities (Cekerevac and Cekerevac, 2025). Such incidents demonstrate that vessel scenarios can generate blast loads sufficient to threaten building integrity and human safety, motivating practical methods to delineate hazard zones for layout design and emergency planning (Stolecka-Antczak et al., 2024; Zhou et al., 2024).

High-fidelity consequence assessment for hydrogen explosions is typically pursued via dedicated experiments and Computational Fluid Dynamics (CFD), but both are costly and time-consuming (Min and Kang, 2024). Commercial integral-model software such as DNV Phast is widely used in industry for explosion consequence analysis, but access can be constrained by licensing requirements and dependence on dedicated software ecosystems (DNV, 2024). As a practical option for early-stage decision-making, the TNT-equivalent approach remains widely applied as a screening method to estimate peak side-on overpressure from scaled-distance relationships for parametric studies, preliminary protection evaluation, and safety-distance determination (Crowl and Louvar, 2011; Han et al., 2025). To address this need, this study developed a web-based hydrogen explosion simulation platform that automates the TNT-equivalent workflow from minimal inputs of inventory volume and evaluation distance. The platform implements three established empirical correlations by Crowl and Louvar, Alonso, and Sadovski under harmonized assumptions and generates peak side-on overpressure as a function of distance. The platform is first validated against instrumented pressure vessel burst datasets reported in the literature to confirm that the predicted overpressure decay with distance is reproduced within the measurement-supported range, and it is subsequently transferred to the Gangneung 2019 case as a field-scale check (Cekerevac and Cekerevac, 2025; CHS, 2019; Han et al., 2025). Following the validation step, the platform provides peak side-on overpressure predictions at the evaluated distances as a preliminary screening output to support early-stage safety-distance interpretation for hydrogen storage scenarios.

METHODOLOGY

A TNT-equivalent method was used to estimate the peak side-on overpressure (P_o) for hydrogen (H_2) explosion scenarios. The three empirical correlations by Crowl and Louvar, Alonso, and Sadovski were implemented within a single computational workflow and executed in parallel under identical scenario inputs (Fig. 1). This allows direct comparison of the predicted overpressure under consistent assumptions. The implementation records the full calculation trail (inputs, intermediate scaled variables, and model-specific outputs) and exports the calculation log in tabular format to support traceability and independent recalculation.

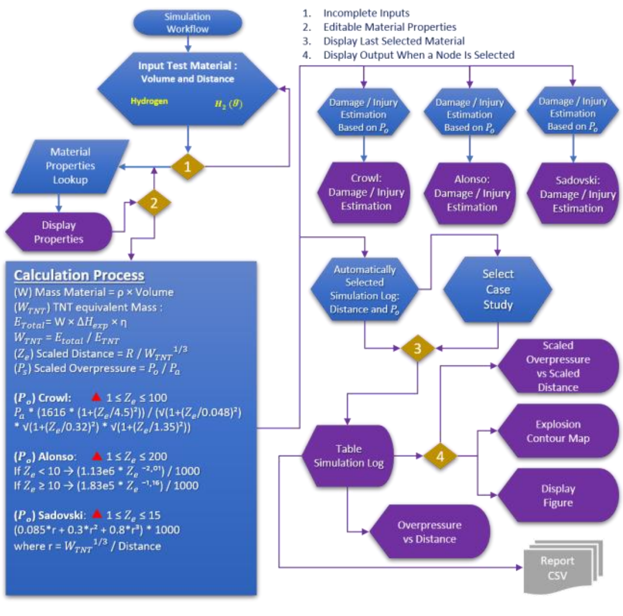

Figure 1. Workflow of the TNT equivalent simulation platform integrating Crowl & Louvar, Alonso, and Sadovski correlations for peak side-on overpressure and consequence estimation

TNT Equivalent Workflow

The inventory mass was determined for each scenario, as determined by Eq. (1).

$$W = \rho \cdot V \quad (1)$$

where W is inventory mass (kg), ρ is density of the inventory ($\mathrm{kg \cdot m^{-3}}$), and V is inventory volume ($\mathrm{m^3}$).

The total energy of the explosive material can be determined using Eq. (2).

$$E_{total} = W \cdot \Delta H_{exp} \cdot \eta \quad (2)$$

where ΔH_{exp} is the explosion energy of the explosive material (with hydrogen's heat of explosion being 130800 kJ/kg) and η is the explosion efficiency factor representing the total energy of the explosive material converted into blast loads. The η value is empirical and contingent upon the conditions of the release of the explosion, ignition sources, and environmental factors. The η value of hydrogen explosions varies from 1% to 10% (Han et al., 2025; Lees, 2012). The equivalent mass of the TNT is calculated based on the total energy released during an explosion using Eq. (3) (Crowl and Louvar, 2011).

$$W_{TNT} = \frac{E_{total}}{E_{TNT}} \quad (3)$$

where W_{TNT} is the TNT equivalent mass (kg), E_{TNT} is the explosion energy of TNT within the range of 4230–4836 kJ/kg (Wang et al., 2023). The W_{TNT} value is utilized to calculate the scaled distance according to the Hopkinson-Cranz scaling law or cube-root law using Eq. (4) (Crowl and Louvar, 2011).

$$Z_e = \frac{R}{W_{TNT}^{1/3}} \quad (4)$$

where Z_e is the scaled distance $\left(\mathrm{m \cdot kg^{-1/3}}\right)$, R is the distance from the explosion center (m). The Hopkinson–Cranz scaling law states that, for a given explosive and detonation configuration, blast overpressure responses are expected to be comparable when evaluated at the same scaled distance, even for different charge weights (Wei and Hargather, 2021).

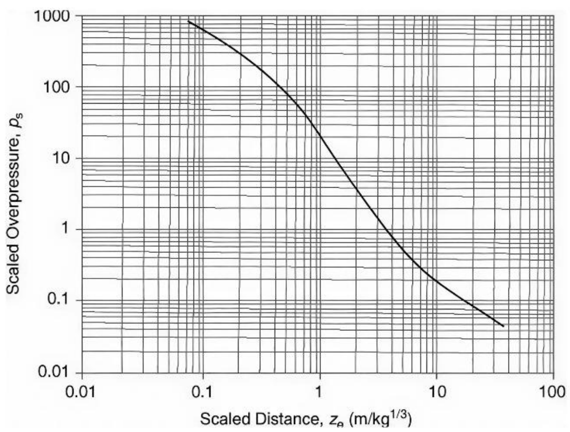

Figure 2. Scaled distance (Z_e) vs scaled overpressure (P_s) for a TNT surface explosion (Crowl and Louvar, 2011)

Scaled overpressure (P_s) is the ratio of peak side-on overpressure (P_o) in kPa to ambient pressure (P_a) of 101.325 kPa, as expressed in Eq. (5) and Fig. 2.

$$P_s = \frac{P_o}{P_a} \quad (5)$$

Empirical Peak Side-on Overpressure Correlations

The three correlations were developed from different experimental bases and therefore differ in applicability range and fitted curve characteristics.

Crowl & Louvar's methodology

Crowl & Louvar (2011) implement the Kinney–Graham correlation for TNT surface bursts on a flat surface, as determined by Eq. (6).

$$\frac{P_o}{P_a} = \frac{1616\left[1+\left(\frac{Ze}{4.5}\right)^2\right]}{\sqrt{\left[1+\left(\frac{Ze}{0.048}\right)^2\right]}\sqrt{\left[1+\left(\frac{Ze}{0.32}\right)^2\right]}\sqrt{\left[1+\left(\frac{Ze}{1.35}\right)^2\right]}} \quad (6)$$

In this study, results at low scaled distances are treated with caution because empirical blast correlations typically show larger dispersion in the near field (e.g., $0.2 \le Z_e \le 1$) and become more stable for $Z_e \ge 1$ (Ullah et al., 2017). Values outside the adopted interpretation range are flagged as extrapolative screening outputs.

Alonso's methodology

The Alonso correlation provides P_o as a power-law function of Z_e over two validity ranges (Díaz Alonso et al., 2006).

For $1 \le Z_e < 10$ can be calculated by Eq. (7) as follows:

$$P_o = 1.13 \times 10^6 \, {Z_e}^{(-2.01)} \quad (7)$$

For $10 \le Z_e \le 200$ can be determined by Eq. (8) as follows:

$$P_o = 1.83 \times 10^5 \, {Z_e}^{(-1.16)} \quad (8)$$

where P_o is obtained in Pascals (Pa) and is converted to kilopascals (kPa) for reporting. Predictions outside $1 \le Z_e \le 200$ are labelled as extrapolated.

Sadovski's methodology

The Sadovski formulation estimates P_o based on empirical TNT blast tests and assumes a pseudo-spherical blast origin(Jeremić and Bajić, 2006), as expressed in Eq. (9).

$$P_o = 0.085\frac{\sqrt[3]{W_{TNT}}}{R} + 0.3\left(\frac{\sqrt[3]{W_{TNT}}}{R}\right)^2 + 0.8\left(\frac{\sqrt[3]{W_{TNT}}}{R}\right)^3 \quad (9)$$

where P_o is obtained in MPa and converted to kPa for reporting. This study applies Sadovski within $1 \le Z_e \le 15$ (Jankura et al., 2020), while values outside this range are flagged as extrapolative.

Consequences Classification Based on Peak Side-on Overpressure

Blast consequences were assessed by mapping the predicted peak side-on overpressure (P_o) to threshold-based structural damage risk and human

Table 1. Summary of structural damage classification thresholds based on peak side-on overpressure

Risk damage	P_o range (kPa)	Short descriptor
RD1 Insignificant	0.14–2	Glazing effects and incidental glass damage
RD2 Minor	>2–9	Minor glass breakage and light architectural damage
RD3 Moderate	>9–25	Widespread glazing failure and major non-structural damage
RD4 Serious	>25–40	Extensive non-structural damage and severe building impairment
RD5 Severe	>40–55	Heavy damage with high likelihood of ceiling and facade collapse
RD6 Major	>55–76	Major damage including impacts to load-bearing components
RD7 Catastrophic	>76	Near-total collapse of building elements

Table 2. Summary of human injury classification thresholds based on peak side-on overpressure

Risk injury	P_o range (kPa)	Short descriptor
RI1 Minor injury	<20	Primary blast injury unlikely, secondary injury possible
RI2 Moderate injury	20–30	Minor contusion and low eardrum-rupture likelihood
RI3 Serious injury	30–50	Injury severity increases due to combined blast and debris effects
RI4 Severe injury	50–100	Severe injury risk with potential fatality depending on exposure
RI5 Fatality	>100	High fatality likelihood for unprotected individuals

injury risk categories (Crowl and Louvar, 2011; Jeremić and Bajić, 2006; Wang et al., 2023).

In this study, classification is reported in terms of P_o as a screening-level metric, consistent with simplified damage criteria that relate peak overpressure to hazard zoning and preliminary safety-distance interpretation. Accordingly, the predicted P_o values at each radial distance were translated into qualitative consequence classes using compiled threshold ranges from multiple literature sources summarised in Tables 1 and 2, while the full classification criteria and source attribution are provided in Supplementary Tables S1 and S2.

Validation Scenarios

Platform performance was evaluated using two complementary validation scenarios, namely a controlled pressure vessel burst dataset and a field benchmark event. The essential input parameters adopted for both cases are summarized in Table 3.

Baseline PVBs scenario

The baseline validation case was adopted from the Type-IV high-pressure hydrogen pressure vessel burst dataset reported by Han et al. (2025), where peak side-on overpressure was measured at distances of 2–18 m from the explosion center and mapped to TNT reference responses with additional refinement using CFD simulations. The dataset represents an open-field configuration, with the ground as the only reflecting boundary. In the reference study, TNT charge weights were designed using an energy-based TNT equivalency framework by considering the commonly reported explosion-efficiency range of 1–10% and selecting three representative values of $\eta = 3.5\%$, 5.5%, and 7.0% to support the experimental matching campaign. Using a hydrogen inventory of 7.15 kg and the adopted energy constants of 130800 kJ/kg for hydrogen and 4520 kJ/kg for TNT, TNT charge weights were evaluated at the same measurement locations as the hydrogen experiment (2, 4, 6, 8, 10, 14, and 18 m) to establish distance-dependent peak overpressure equivalence. Following the experimental–computational matching, a calibrated TNT-equivalent mass of 9.53 kg with a corresponding yield factor of 0.046 was reported, and these calibrated parameters were adopted directly in this study so that the platform inputs rely on a measurement-anchored TNT equivalency rather than an assumed or tuned efficiency.

For thermophysical consistency, hydrogen properties were evaluated in Aspen HYSYS using the hydrogen-suitable MBWR package as the equation of state (Rezaie Azizabadi et al., 2021). The inventory density was taken from the reported vessel charge ($\rho = 40.86$ kg/m³) and cross-checked at the rupture pressure (79.8 MPa) in Aspen HYSYS v14 (Aspen Technology, Inc., 2023) using MBWR. The bulk temperature was iteratively adjusted until the EOS reproduced the inventory-based density, yielding an EOS-consistent state of T = 46.86 °C with a non-ideal compressibility factor of $Z = 1.4$.

Field-scale case (R&D Gangneung 2019)

After validation against the PVBs dataset, the platform was further assessed using the hydrogen tank explosion that occurred in Gangneung, South Korea, in May 2019 as a field-scale case. A technical review by the Center for Hydrogen Safety estimated the event to be equivalent to approximately 50 kg TNT and reported no secondary fire, indicating that the observed consequences were primarily blast driven. The same review described severe near-field damage at around 15 m and widespread window breakage at approximately 100 m (CHS, 2019). In this study, the Gangneung scenario was represented using the reported tank capacity and operating pressure together with ambient conditions, with the ambient temperature taken as approximately 31°C based on historical weather records for Gangneung in May 2019 (timeanddate.com, 2019).

Table 3. Validation scenarios for hydrogen explosions, including essential input parameters

Properties	H_2 explosion experiment (Han et al., 2025)	R&D Gangneung H_2 tank explosion (Cekerevac and Cekerevac, 2025; CHS, 2019)
Density, $\boldsymbol{\rho}$ $(\boldsymbol{kg/m^3})$	40.86	0.793
Volume, V $(\boldsymbol{m^3})$	0.175	40
Heat of explosion, $\boldsymbol{\Delta H_{exp}}$ $(\boldsymbol{kJ/kg})$	130800	130800
Explosion energy of TNT, $\boldsymbol{E_{TNT}}$ $(\boldsymbol{kJ/kg})$	4520	4520
Efficiency ($\boldsymbol{\eta}$)	0.046	0.055

Hydrogen density at 1 MPa and the adopted ambient temperature was cross-checked in Aspen HYSYS v14 (Aspen Technology, Inc., 2023) using the hydrogen suitable MBWR package, yielding $\rho = 0.793$ kg/m³ with a near-ideal compressibility factor of Z = 1.006. To preserve consistency with the baseline energy-based TNT-equivalency framework, the explosion efficiency for the Gangneung case was not introduced as an independent tuning parameter. Instead, the efficiency was back calculated as 0.055 (5.5%) so that the reported field equivalence of 50 kg TNT is reproduced under the adopted hydrogen inventory and the same energy constants used in the baseline case.

RESULTS AND DISCUSSION

Pressure Vessel Bursts (PVBs) Baseline Validation

Peak side-on overpressure data for the baseline PVB validation in this study was adopted from the Type-IV hydrogen pressure vessel burst experiments reported by Han et al. (2025). The measured response exhibits a pronounced decay with distance, decreasing from 1238.98 kPa at $R = 2$ m to 23.17 kPa at $R = 18$ m. The reference study also noted near-field measurement limitations, where the 2 m and 4 m sensors were damaged after capturing the peak overpressure value, resulting in comparatively noisier signals at these locations than at the remaining measurement points.

As summarized in Table 4, the three TNT-equivalent equations (Crowl and Louvar, Alonso, and Sadovski) reproduce the distance-dependent attenuation of measured peak side-on overpressure, while the predicted pressure levels differ across evaluation distances. At $R = 2$ m ($Z_e = 0.94$), Crowl and Louvar equation yields a markedly higher estimate (2287.41 kPa, +85%), whereas Alonso equation provides the closest agreement (1270.59 kPa, +3%) and Sadovski gives 1380.24 kPa (+11%). At $R = 4$ m ($Z_e = 1.89$), Crowl and Louvar remain above the measurement (+18%), while Alonso and Sadovski equations underpredict (−22% and −38%). Over the sensor-intact window of 6–18 m, Crowl and Louvar equation continues to overpredict but with a progressively smaller deviation (+42% at 6 m to +8% at 18 m), whereas Alonso and Sadovski are predominantly below the measurements and converge to similar values at the longest evaluation distance (−34% and −33% at 18 m). These pointwise deviations indicate that, under harmonized TNT-equivalent inputs, screening distances inferred at a specified P_o criterion can vary across formulations.

As shown in Fig. 3, the platform-generated baseline-validation visualizations present both scaled-distance coordinates and peak overpressure versus evaluation distance, enabling cross-correlation differences to be examined on a consistent TNT-equivalent basis. Across the evaluated window, inter-model dispersion is more pronounced at lower scaled distances ($0.2 < Z_e < 1.0$), and whereas the variation becomes much smaller for $Z_e > 1.0$, indicating that the empirical relations tend to converge more closely in the larger-scaled-distance regime (Ullah et al., 2017). In the present dataset, only the $R = 2$ m point yields $Z_e < 1$, whereas the remaining points ($R =$ 4–18 m) correspond to $Z_e > 1$, consistent with tighter clustering of predictions as Z_e increases. Accordingly, the platform applies Z_e-based validity alarms and prioritizes screening interpretation in the higher-Z_e regime, while results at lower Z_e are interpreted with additional caution. This treatment aligns with broader discussions that TNT-equivalent screening tends to be more dependable at larger distances,

Table 4. Deviation of TNT-equivalent predictions from measured peak side-on overpressure in the Type-IV hydrogen PVBs case

Distance, R (m)	$\boldsymbol{P_o}$, exp (kPa)	$\boldsymbol{Z_e}$ (m·kg$^{-1/3}$)	Crowl & Louvar		Alonso		Sadovski	
			P_o (kPa)	Error (%)	P_o (kPa)	Error (%)	P_o (kPa)	Error (%)
2	1238.98	0.94	2287.412	85	1270.585	3	1380.244	11
4	403.57	1.89	476.485	18	315.452	-22	248.461	-38
6	132.37	2.83	187.462	42	139.634	5	102.791	-22
8	79.26	3.77	100.973	27	78.318	-1	58.488	-26
10	56.25	4.72	65.132	16	50.012	-11	39.13	-30
14	33.19	6.6	36.387	10	25.431	-23	22.531	-32
18	23.17	8.49	24.966	8	15.345	-34	15.481	-33

Notes: (1) Positive error indicates overprediction; (2) negative error indicates underprediction

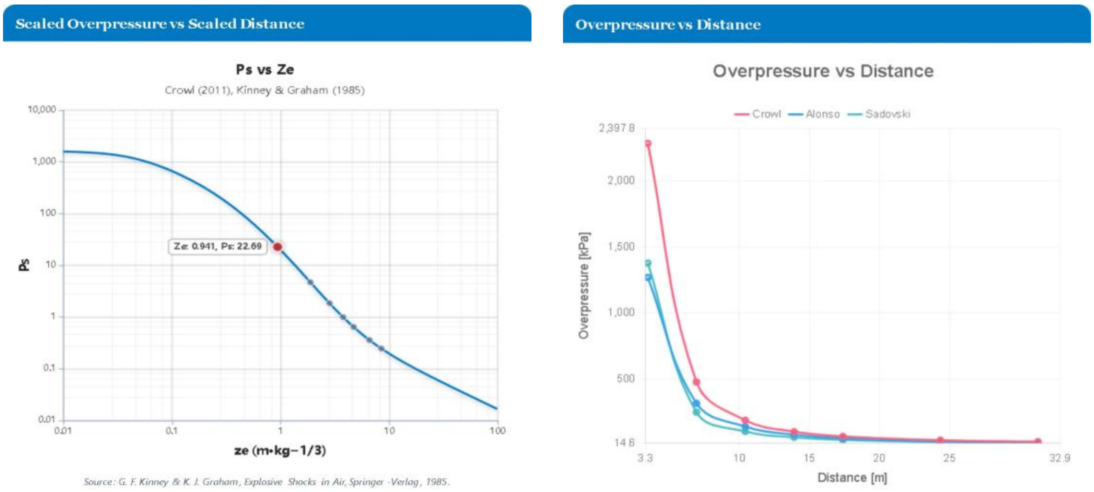

(a) Scaled overpressure as a function of scaled distance

(b) Predicted peak side-on overpressure versus distance or cross-correlation comparison.

Figure 3. Platform-generated baseline PVBs validation visualization against Type-IV hydrogen pressure vessel burst measurements

whereas close-range predictions are more sensitive to uncertainties in the effective source representation and the fraction of release energy converted into blast loading (Chen et al., 2023).

Overall predictive performance over the evaluation window was summarized using the mean absolute error (MAE) and the coefficient of determination (R^2). MAE quantifies the average absolute deviation between measured and predicted peak side-on overpressures, whereas R^2 indicates how well the models reproduce the distance-dependent attenuation pattern across the evaluated distances. Because MAE is based on absolute deviations, it does not retain the sign of the residuals; therefore, the direction of the pointwise errors reported in Table 4 was examined in parallel when interpreting conservatism for screening applications (Khoshvaght et al., 2025). The statistics were calculated over the sensor-intact window of 6–18 m (6, 8, 10, 14, and 18 m) to remain consistent with the reliability window adopted in the reference dataset and to avoid overweighting the close-range regime. For each evaluation distance, the measured value is denoted by $y_i$and the corresponding model prediction is denoted by x_i. MAE was calculated as the average absolute deviation across n distances (Eq. 10), and R^2 was calculated from the residual and total sums of squares (Eq. 11), where $\bar{y}$ denotes the meaning of the measured values.

$$MAE = \frac{1}{n}\sum_{i=1}^{n}|y_i - x_i| \quad (10)$$

$$R^2 = 1 - \frac{\sum_{i=1}^{n}(y_i - x_i)^2}{\sum_{i=1}^{n}(y_i - \bar{y})^2} \quad (11)$$

Over 6–18 m, Alonso equation gives the lowest MAE (6.006 kPa) with $R^2 = 0.999$, while Crowl and Louvar and Sadovski equations yield MAEs of 18.136 kPa and 17.164 kPa with R^2 values of 0.985 and 0.993, respectively. The uniformly high R^2 values confirm that all three correlations represent the attenuation pattern well over the evaluated window; the practical distinction is therefore dominated by magnitude agreement and error direction. In this dataset, Crowl and Louvar equation provides consistently higher estimates over 6–18 m with decreasing deviation at larger distances, supporting its use as a conservative screening curve, whereas Alonso equation provides the closest numerical agreement but remains below the measurements at several $Z_e > 1$ points and is therefore better positioned as a best-fit reference or as a comparative curve alongside a conservative envelope.

Transferability of the Calibrated PVBs Baseline to a Real Event: Gangneung 2019

The calibrated PVB baseline was transferred to the Gangneung 2019 field-scale case by matching the Hopkinson–Cranz scaled distance (Z_e), so that comparable blast overpressure responses are inferred on a consistent TNT-equivalent basis. Under this principle, blast responses from different charge weights can be compared when evaluated at the same scaled distance (Wei and Hargather, 2021).

In this study, the Gangneung 2019 incident was represented as a field-scale case with an estimated equivalence of approximately 50 kg TNT, with consequences dominated by blast effects and without a dominant secondary fire. By retaining the baseline Z_e values, each baseline radial evaluation distance (R) was mapped to an adjusted field distance (R_{adj}) for the 50 kg charge using Eq. (12). This mapping yields some correspondence from 2–18 m in the baseline case to approximately 3.48–31.30 m as shown in Supplementary Table S3.

$$R_{adj} = Z_e \cdot W_{TNT}^{1/3} \quad (12)$$

The mapped field distances and the corresponding peak side-on overpressures predicted by Crowl & Louvar, Alonso, and Sadovski equations are reported in Supplementary Table S3. Internal scale

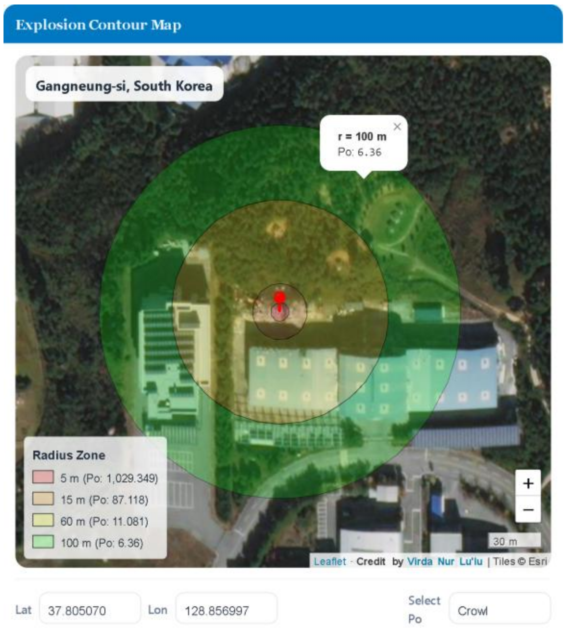

(a) Platform-generated peak side-on overpressure (P_o) contour map for the Gangneung 2019 case (50 kg TNT equivalent)

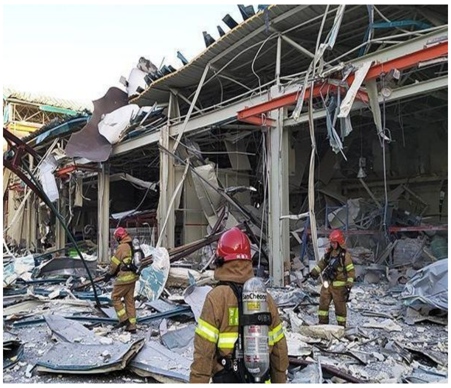

(b) Near-field structural damage observed at approximately 15 m

(c) Far-field facade damage observed at approximately 100 m

Figure 4. Field-scale consequence interpretation for the Gangneung 2019 benchmark at 50 kg TNT equivalent (Lim, 2019; The Korea Times, 2019)

scale-transfer consistency was verified by comparing predictions at identical scaled distances between the calibrated PVB baseline and the 50 kg TNT-equivalent Gangneung 2019 case. Across all mapped points and correlations, deviations remained within −0.27% to 0.10%, indicating that the cube-root scaling implementation was numerically consistent, with residual differences attributable to rounding and floating-point precision. These deviations are well below the 1% magnitude commonly reported for simulator-to-benchmark comparisons in chemical engineering, supporting internal consistency of the scale-up implementation (Andreasen, 2022).

Consequence Interpretation Based on Structural and Human-Injury Thresholds

Following verification of the scale-transfer consistency, the predicted peak side-on overpressure for the Gangneung 2019 case (TNT-equivalent mass of 50 kg) was interpreted using threshold-based consequence zoning. Predictions from Crowl and Louvar, Alonso, and Sadovski equations were mapped to the structural damage risk categories in Table 1 (RD1–RD7) and the human injury risk categories in Table 2 (RI1–RI5). The three correlations are presented in parallel to quantify inter-correlation spread, while a conservative zoning interpretation is obtained by referencing the upper-bound P_o at each evaluation distance to avoid delineating buffer zones using lower estimates. The spatial distribution of P_o is additionally summarized by the platform-generated contour map in Fig. 4(a), where the source location is specified by input coordinates (37.805070° N, 128.856997° E) adopted from the R&D Gangneung site marker in Google Maps; this coordinate input places the explosion center on the basemap so that contour zones can be interpreted directly against evaluation distances.

Consistency with reported field effects was assessed using two qualitative indicators documented by the Center for Hydrogen Safety, namely structural steel member deformation at approximately 15 m and extensive window breakage at approximately 100 m (CHS, 2019), supported by post-incident photographs in Fig. 4(b)–(c). At 15 m ($Z_e = 4.06$ m·kg$^{-1/3}$), the predicted overpressure is 51.1 kPa (Sadovski equation), 67.6 kPa (Alonso equation), and 87.1 kPa (Crowl and Louvar equation), mapping to RD5–RD7 in Table 1. This band corresponds to severe-to-catastrophic structural damage risk categories, which is compatible with the reported deformation of steel members at that distance; within the three predictions, Alonso falls within the RD6 interval while Crowl and Louvar equation provides the conservative envelope (RD7). At 100 m ($Z_e = 27.06$ m·kg$^{-1/3}$), predicted overpressure decreases to 6.36 kPa (Crowl and Louvar equation), 3.99 kPa (Alonso equation), and 3.59 kPa (Sadovski equation), mapping to RD2 in Table 1, a regime dominated by facade and glazing damage rather than load-bearing failure, consistent with the reported widespread window breakage. For this distance, the platform flags the Sadovski equation result as extrapolative because Z_e exceeds its stated validity range; therefore, interpretation can preferentially reference Alonso equation for alignment with the correlation's validity window while retaining Crowl and Louvar equation as the conservative upper bound for buffer-zone screening.

For human-injury interpretation, the 15 m predictions (51.1–87.1 kPa) map to RI4 in Table 2 (50–100 kPa), which denotes a severe-injury regime with potential fatality for unprotected exposure under peak-overpressure threshold schemes (Crowl and Louvar, 2011; Jeremić and Bajić, 2006; Wang et al., 2023). At 100 m, the predicted peak side-on overpressures (3.6–6.4 kPa) remain within RI1 (<20 kPa), where primary blast injury is unlikely; consequence interpretation is therefore driven mainly by secondary/tertiary injury pathways associated with facade and glazing damage, consistent with the RD2 structural classification at the same distance. Public reporting of the Gangneung incident indicates fatalities and injuries but does not provide verified exposure distances; accordingly, the injury discussion in this study is presented as a threshold-based check for zoning interpretation, rather than a distance-calibrated validation of casualty outcomes.

CONCLUSION

This study delivers a web-based simulation platform that automates a transparent TNT-equivalent workflow for hydrogen consequence screening, enabling traceable calculation from inventory inputs to Hopkinson–Cranz scaling and peak side-on overpressure prediction using multiple empirical correlations. Internal verification of the scale-transfer implementation from the calibrated pressure-vessel-burst baseline to the Gangneung 2019 case shows deviations limited to −0.27% to 0.10%, confirming numerically consistent implementation with differences mainly attributable to precision and rounding.

Against the Type-IV hydrogen pressure vessel burst dataset, all correlations reproduce the attenuation pattern over the sensor-intact 6–18 m window. The Alonso equation provides the closest agreement (MAE 6.006 kPa; R^2 0.999), whereas Crowl and Louvar equation yields higher estimates with decreasing deviation at larger evaluation distances. This supports the use of Crowl and Louvar equation as a conservative screening envelope when buffer-zone definition should avoid reliance on lower predictions.

For the Gangneung 2019 case, predicted overpressures at approximately 15 m correspond to major-to-catastrophic structural damage risk categories and a severe injury band for unprotected exposure, while values at approximately 100 m fall within a glazing-dominated damage regime with a low likelihood of primary blast injury but credible secondary injury potential from glass fragments.

For common explosive-chemical scenarios that can be represented using a TNT-equivalent mass, the three empirical correlations should be used according to their screening roles and scaled-distance applicability. The Crowl and Louvar equation is recommended for conservative preliminary screening when separation-distance or buffer-zone estimation should avoid underprediction. The Alonso equation is suitable as a best-estimate reference when the evaluated scenario remains within its validity range and validation data indicates close agreement. The Sadovski correlation can be used as an additional comparative model within its stated validity range, but extrapolated results should be clearly flagged and should not be used as the sole basis for safety-distance determination.

Future work will prioritize strengthening the screening credibility of the TNT-equivalent platform through broader multi-scenario validation for hydrogen explosions using additional instrumented datasets and field benchmarks, supported by a structured parameter database for key assumptions, particularly the case-dependent efficiency factor, to enable sensitivity- and uncertainty-aware screening outputs. The platform framework will then be extended to additional hazardous materials so that cross-material consequence screening can be performed under harmonized assumptions and consistent reporting.

CONFLICT OF INTEREST

The authors confirm that there are no conflicts of interest.

ACKNOWLEDGEMENTS

The authors acknowledge the published datasets and incident reports that enabled the validation framework used in this study.

REFERENCES

Andreasen, A., (2022). Evaluation of an open-source chemical process simulator using a plant-wide oil and gas separation plant flowsheet model as basis. *Periodica Polytechnica Chemical Engineering*, 66(3), pp.503–511. https://doi.org/10.3311/PPch.19678

Aspen Technology, Inc., (2023). *Aspen HYSYS v14*. Aspen Technology, Inc.

Calabrese, M., Portarapillo, M., Di Nardo, A., Venezia, V., Turco, M., Luciani, G. and Di Benedetto, A., (2024). Hydrogen safety challenges: a comprehensive review on production, storage, transport, utilization, and CFD-based consequence and risk assessment. *Energies*, 17(6), p.1350. https://doi.org/10.3390/en17061350

Cekerevac, Z. and Cekerevac, D., (2025). Hydrogen hazards, risks, and protection: an in-depth review. *MEST Journal*, 13, pp.23–48. https://doi.org/10.12709/mest.13.13.SP.02

Center for Hydrogen Safety (CHS), (2019). Review: hydrogen tank explosion in Gangneung, South Korea. Presented at the 2019 Center for Hydrogen Safety Conference, AIChE (American Institute of Chemical Engineers).

Chen, D., Wu, C. and Li, J., (2023). Assessment of modeling methods for predicting load resulting from hydrogen-air detonation. *Process Safety and Environmental Protection*, 180, pp.752–765. https://doi.org/10.1016/j.psep.2023.10.051

Crowl, D.A. and Louvar, J.F., (2011), *Chemical Process Safety: Fundamentals with Applications*, 3rd ed., Prentice Hall, Upper Saddle River, New Jersey.

Díaz Alonso, F., González Ferradás, E., Francisco Sánchez Pérez, J., Miñana Aznar, A., Ruiz Gimeno, J. and Martínez Alonso, J., (2006). Characteristic overpressure–impulse–distance curves for the detonation of explosives, pyrotechnics or unstable substances. J*ournal of Loss Prevention in the Process Industries*, 19(6), pp.724–728. https://doi.org/10.1016/j.jlp.2006.06.001

DNV, (2024). *Phast: Fire, Explosion, Dispersion, and Toxic Modeling Software*. DNV. Available at: https://www.dnv.com/

DNV, (2026). *Energy Transition Outlook 2026: Hydrogen to 2060*. DNV AS. Available at: https://www.dnv.com/publications/energy-transition-outlook-2026-hydrogen-to-2060/

Han, S., Baek, S.-H., Jeon, Y., Kim, K. and Park, S., (2025). Integrated experimental-computational approach to estimate TNT equivalence of hydrogen vessel bursts. *International Journal of Hydrogen Energy*, 146, p.149936. https://doi.org/10.1016/j.ijhydene.2025.06.126

International Energy Agency (IEA), (2025). *Global Hydrogen Review 2025*. International Energy Agency, Paris. Available at: https://www.iea.org/reports/global-hydrogen-review-2025/executive-summary

Jankura, R., Zvaková, Z. and Boroš, M., (2020). Analysis of mathematical relations for calculation of explosion wave overpressure. *Proceedings of CBU in Natural Sciences and ICT*, 1, pp.21–27. https://doi.org/10.12955/pns.v1.116

Jeremić, R., Bajić, Z., (2006). An approach to determining the TNT equivalent of high explosives. *Scientific Technical Review*, LV, pp.58–62.

Joshi, A., Sattari, F., Lefsrud, L., Tufail, M. and Khan, M.A., (2024). Mitigating uncertainty: A risk informed approach for deploying hydrogen refueling stations. *International Journal of Hydrogen Energy*, 74, pp.136–150. https://doi.org/10.1016/j.ijhydene.2024.06.085

Khoshvaght, H., Permala, R.R., Razmjou, A. and Khiadani, M., (2025). A critical review on selecting performance evaluation metrics for supervised machine learning models in wastewater quality prediction. *Journal of Environmental Chemical Engineering*, 13, p.119675. https://doi.org/10.1016/j.jece.2025.119675

LaChance, J., (2009). Risk-informed separation distances for hydrogen refueling stations. *International Journal of Hydrogen Energy*, 34, pp.5838–5845. https://doi.org/10.1016/j.ijhydene.2009.02.070

Lees, F., (2012), *Lees' Loss Prevention in the Process Industries*, 4th ed., Elsevier, Amsterdam.

Lim, C.-W., (2019). Explosion at hydrogen fuel-cell power system kills two and injuries six others. *AJP News Agency*. Available at: https://www.ajupress.com/view/20190524113435564

Ma, Q., Guo, Y., Zhong, M., Ya, H., You, J., Chen, J. and Zhang, Z., (2024). Numerical simulation of hydrogen explosion characteristics and disaster effects of hydrogen fueling station. *International Journal of Hydrogen Energy*, 51, pp.861–879. https://doi.org/10.1016/j.ijhydene.2023.05.129

Min, H. and Kang, H., (2024). Prediction of a hydrogen vapor cloud explosion with a barrier wall using various machine learning methods. *Processes,* 12(12), p.2946. https://doi.org/10.3390/pr12122946

Rezaie Azizabadi, H., Ziabasharhagh, M. and Mafi, M., (2021). Applicability of the common equations of state for modeling hydrogen liquefaction processes in Aspen HYSYS. *Gas Processing Journal*, 9. https://doi.org/10.22108/gpj.2020.123736.1087

Stolecka-Antczak, K., Rusin, A., Kosman, W., Rusin, K. and Paltrinieri, N., (2024). Hazards caused by hydrogen explosion at refueling station due to uncontrolled gas release. In: Kołowrocki, K. and Dąbrowska, E., eds., *Advances in Reliability, Safety and Security: ESREL 2024 Contributions*, Part 1. Polish Safety and Reliability Association, pp.231–240. https://esrel2024.com/wp-content/uploads/articles/part1/hazards-caused-by-hydrogen-explosion-at-refueling-station-due-to-uncontrolled-gas-release.pdf

Suwa, Y., (2024). Studies on the safe application techniques of high-pressure hydrogen gas. *Journal of Physics: Conference Series*, 2812, p.012002. https://doi.org/10.1088/1742-6596/2812/1/012002

The Korea Times, (2019). Hydrogen tank explosion kills 2 in Gangneung. *The Korea Times*. Available at: https://www.koreatimes.co.kr/southkorea/society/20190523/hydrogen-tank-explosion-kills-2-in-gangneung

timeanddate.com, (2019). Past Weather in Gangneung, South Korea — May 2019. Available at: https://www.timeanddate.com/weather/south-korea/gangneung/historic?month=5&year=2019

Ullah, A., Ahmad, F., Jang, H.-W., Kim, S.-W. and Hong, J.-W., (2017). Review of analytical and empirical estimations for incident blast pressure. *KSCE Journal of Civil Engineering*, 21, pp.2211–2225. https://doi.org/10.1007/s12205-016-1386-4

Wang, Q., Zhang, L., Wang, L. and Bu, L., (2023). A practical method for predicting and analyzing the consequences of ammonium nitrate explosion accidents adjacent to densely populated areas. *Heliyon*, 9, e15616. https://doi.org/10.1016/j.heliyon.2023.e15616

Wei, T. and Hargather, M.J., (2021). A new blast wave scaling. *Shock Waves*, 31, pp.231–238. https://doi.org/10.1007/s00193-021-01012-y

Yang, F., Wang, T., Deng, X., Dang, J., Huang, Z., Hu, S., Li, Y. and Ouyang, M., (2021). Review on hydrogen safety issues: incident statistics, hydrogen diffusion, and detonation process. *International Journal of Hydrogen Energy*, 46, pp.31467–31488. https://doi.org/10.1016/j.ijhydene.2021.07.005

Zhou, Y., Huang, L., Li, Y. and Gao, W., (2024). The prediction model for explosion overpressure in unconfined hydrogen cloud explosion. *Journal of Loss Prevention in the Process Industries*, 88, p.105254. https://doi.org/10.1016/j.jlp.2024.105254